Chin. J. Astron. Astrophys. Vol. 7 (2007), No. 5, 657–668
(*http://www.chjaa.org*)

Chinese Journal of
Astronomy and
Astrophysics

An Infrared Photometric Study of Galaxies with Extragalactic H_2O Maser Sources *

Pei-Sheng Chen, Yi-Fei Gao and Hong-Guang Shan

National Astronomical Observatories / Yunnan Observatory, Chinese Academy of Sciences, Kunming 650011; *iraspsc@yahoo.com.cn*

Received 2006 October 15; accepted 2006 December 1

Abstract All galaxies with extragalactic H_2O maser sources observed so far are collected. With the 2MASS and the IRAS photometric data an infrared study is performed on those galaxies. By a comparison between the H_2O maser detected sources and non-detected sources in the infrared it is indicated that infrared properties in the IRAS 12–25 μm and 60–100 μm are important for producing H_2O masers in galaxies. It is also found that the H_2O maser galaxies with different nuclear activity types have rather different infrared properties mainly in the IRAS 12–60 μm region.

Key words: galaxies: maser — galaxies: nuclei — galaxies: starburst — infrared: galaxies

1 INTRODUCTION

The discovery of H_2O masers in our Galaxy has prompted searches for similar masers in extragalactic sources. The first extragalactic H_2O maser in M33 was found 30 years ago, the so called H_2O kilo-maser (Churchwell et al. 1977), whose maser luminosity is compatible to that of our Galactic H_2O masers. After only 2 years the first H_2O mega-maser was found in NGC 4945 (Dos Santos et al. 1979), so named because its luminosity is as high as 10^6 times more powerful than that of typical strong Galactic H_2O masers. Since then, many attempts to search for more H_2O masers in extra-galaxies have been made by using either single dish radio telescopes of appropriate size or the VLBI at 22.235 GHz (Elitzur 1992; Lo 2005). As of date the number of H_2O masers in extra-galaxies including both the kilo-masers and the mega-masers stands at about 70 (Lo 2005 and references therein).

It is likely that most H_2O kilo-masers are physically associated with enhanced star formation and starbursts in the extended regions of their parent galaxies. While some H_2O kilo-masers are powered by AGNs, most H_2O mega-masers are located in the innermost few parsecs, powered by the central AGNs and associated with Seyfert 2 or LINER nuclei. Then most H_2O mega-maser activities are related to the large line-of-sight column densities expected when the nuclear tori are viewed edge-on (e.g. Henkel et al. 2003; Lo 2005).

There is evidence for a total of three distinct classes of extragalactic H_2O masers: (1) Accretion disk mega-masers, that are located within the central pc of molecular accretion disks. These masers allow us to map the nuclear accretion disks, to determine the nuclear masses and accurate distances to their parent galaxies, thus having an impact on the cosmic distance scale; (2) Jet mega-masers that are at least partly the results of interaction between nuclear radio jets and encroaching molecular clouds within tens of pc of the center. Monitoring the line and continuum fluxes can provide estimates of the speed of the material in the jet through reverberation mapping. (3) Kilo-masers with typically lower maser luminosities often associated with prominent star forming regions in large scale galactic disks. This kind of masers can be used to pinpoint

* Supported by the National Natural Science Foundation of China.

locations of high mass star formation and to determine the distances through complementary measurements of proper motions and radial velocities (Schulz et al. 2003; Henkel et al. 2004; Lo 2005; Tarchi et al. 2006).

So far, about 1000 active galaxies have been surveyed for extragalactic H_2O masers, but only about 70 were found to contain these. The low detection rates are probably the result of the limited sensitivities of the surveys, rather than an intrinsic lack of extragalactic H_2O masers (Henkel et al. 2005; Lo 2005). Although it is now believed that the seed radio photons and X-ray photons produced from the central AGNs of the galaxies can pump the H_2O masers through collisions (Falcke et al. 2000; Lo 2005), hot young stars (particularly for the kilo-masers) are probably the ultimate power source of the pump and infrared emission (Gardner et al. 1982).

It should be emphasized that extragalactic H_2O masers are preferentially detected in nearby galaxies that are bright in the mid- and far-infrared (Braatz et al. 1997; Tarchi et al. 2002a). Furthermore, it is believed that the far-infrared radiations from cold dust and gas are trapped and absorbed by the H_2O molecules, allowing for a much larger region where the population inversion is not quenched and remains constant with increasing optical depth, thereby accounting for the large luminosity observed in the extragalactic H_2O masers (Collison et al. 1995; Lo 2005). Infrared radiations may thus play an important role for producing the H_2O masers.

In this paper all galaxies with extragalactic H_2O masers known so far are collected and their counterparts in the 2MASS and the IRAS observations are identified. From the 2MASS and IRAS observations the infrared photometric properties of those galaxies with extragalactic H_2O masers are discussed.

2 WORKING SAMPLE AND DATA PROCESSING

2.1 Working Sample

The number of galaxies with extragalactic H_2O masers observed so far totals 70, and these are listed in Braatz's web site (Lo 2005, hereafter the Braatz Catalog) which we take as is our basic working sample.

2.2 Identification of 2MASS and IRAS Counterparts

The positions given in the Braatz Catalog are from different sources that are basically inhomogeneous. In order to avoid such inhomogeneity and make the cross-identifications with the 2MASS more secure, we first made positional corrections to all the entries in the Braatz Catalog with the USNO-B1.0 Catalog (Monet et al. 2003, hereafter USNO) because the latter has typical positional uncertainties less than 1 arcsec, then the corrected positions were used to make the cross-identifications with the positions given in the 2MASS Point Source Catalog (2MASS Home Page 2003, Available from: *http://pegasus.phast.umass.edu/*, hereafter 2MASS PSC), taking the 7 arcsec of the maximum positional uncertainty in the 2MASS PSC as the upper limit of a cross-identification. In fact, all the USNO positions for our target galaxies were never more than 2 arcsec away from the 2MASS positions, which shows that the cross-identifications were reliable. Finally 68 out of the 70 galaxies with the extragalactic H_2O masers were found to have 2MASS counterparts.

In the original IRAS Point Source Catalog (IRAS PSC) and IRAS Faint Source Catalog (IRAS FSC) the positional errors for sources usually are as large as $10'' - 30''$ (IRAS Explanatory Supplement 1988, hereafter IRAS ES). Fortunately, in the IRAS PSC/FSC the 95% confidence positional error ellipse for each source is given (IRAS ES). Therefore, if the position of a galaxy with extragalactic H_2O maser from the USNO is located within the corresponding IRAS error ellipse, then the cross-identification is certain. If within the positional error ellipse of the IRAS source there are more than one source besides the one with extragalactic H_2O maser, then information from the Simbad database and the CDS VizieR is taken into account to make the proper identification. Finally out of the 70 galaxies with extragalactic H_2O masers 63 were found to have IRAS PSC or FSC counterparts.

The magnitudes with the uncertainties in the JHK bands from the 2MASS PSC and the flux densities at 12, 25, 60 and 100 μm in Jy from the IRAS PSC/FSC are listed for our targets in Table 1.

The columns of Table 1 are as follows: (1) source number from the Braatz Catalog; (2) source name from the Braatz Catalog; (3) type of nuclear activity from the Braatz Catalog or from Zhang et al. (2006), or from the Simbad database: SBG, Starburst galaxy; S1, Seyfert 1; S2, Seyfert 2; LINER, Low-ionization nuclear emission line region; FRII, Fanarov-Riley type II galaxy; ULIRG, Ultraluminous infrared galaxy; C: Compton-thick; X-, X-ray source in the absence of a starburst and a prominent nuclear source. The symbol "*" indicates that the type is from the Simbad database; (4) redshift from the Simbad database;

Table 1 Infrared Properties of Galaxies with Extragalactic H_2O Masers

No.	Source Name	Type	z	RA	Dec	J	e_J	H	e_H	K	e_K	IRASPSC/FSC	F_{12}	F_{25}	F_{60}	F_{100}	Note
(1)	(2)	(3)	(4)	(5)	(6)	(7)	(8)	(9)	(10)	(11)	(12)	(13)	(14)	(15)	(16)	(17)	(18)
1	IC10 (a)	X–1	0.0012	002017.39	+591839.8	15.266	0.073	14.676	0.113	13.796	0.072	00175+5902	0.406	2.793	/	29.2	Henkel86,#
	IC10 (b)	X–1	0.0012	002027.01	+591736.4	13.201	/	14.582	0.108	12.402	/	00177+5900	0.820	3.749	31.23	71.2	Henkel86,#
2	NGC 235A	S2	0.0222	004252.80	–233227.7	12.584	0.076	11.918	0.100	11.199	0.044	/	/	/	/	/	Kondratko03, 06
3	NGC 253	SBG	0.0008	004733.07	–251719.0	11.233	0.142	10.001	0.180	8.639	0.072	F00450–2533	2.402	11.97	78.42	99.3	Ho87,#
4	Mrk 348	S2	0.0151	004847.15	+315725.1	12.954	0.049	12.304	0.079	11.546	0.051	F00460+3141	0.308	0.835	1.290	1.55	Falcke00
5	ESO 013-G012	S2	0.0168	010702.19	–801828.2	14.053	0.187	12.880	0.202	11.306	/	F01063–8034	0.164	0.143	1.517	6.51	Greenhill02
6	Mrk 1	S2	0.0160	011607.21	+330521.6	13.790	0.064	13.090	0.101	12.598	0.062	F01133+3249	/	0.865	2.531	2.92	Braatz94
7	M33 IC 133	X–8	0.0006	013316.54	+305249.8	15.766	0.070	15.175	0.098	14.282	0.060	F01304+3037	0.270	2.692	10.38	7.36	Churchwell77,#
	M33 IC 342	X–8	0.0006	013330.01	+303145.6	14.859	0.046	14.018	0.048	13.566	0.046	/	/	/	/	/	Huchtmeier78,#
8	NGC 591	S2	0.0151	013331.23	+354005.6	12.958	0.055	12.237	0.052	11.865	0.043	F01306+3524	0.155	0.448	1.991	3.48	Braatz04
9	NGC 613	S	0.0049	013418.19	–292506.5	11.645	0.081	11.125	0.105	10.376	0.073	F01319–2940	0.997	2.447	22.01	50.0	Kondratko03,06
10	IC 0184	S2	0.0180	015951.23	–065025.3	13.335	0.045	12.652	0.055	12.414	0.063	F01573–0704	/	/	0.913	0.913	Kondratko06
11	NGC 1052	LINER	0.0049	024104.79	–081520.9	11.006	0.084	10.404	0.120	9.811	0.063	02386–0828	/	0.501	0.938	1.51	Braatz94
12	NGC 1068	S2,C	0.0038	024240.71	–000048.0	10.179	0.104	9.136	0.121	7.271	0.024	02401–0013	38.30	86.83	185.8	224.0	Claussen84, Braatz96
13	Mrk 1066	S2,C	0.0121	025958.60	+364913.7	11.862	0.025	10.966	0.021	10.729	0.026	F02568+3637	0.447	2.263	1.098	12.1	Henkel05
14	0335+0104	S2*	0.0399	033810.38	+011418.3	14.499	0.060	13.774	0.055	13.338	0.060	F03355+0104	/	0.419	0.591	/	Kondratko03
15	NGC 1386	S2,C	0.0029	033646.20	–355957.3	11.578	0.090	10.827	0.114	10.260	0.061	F03348–3609	0.493	1.433	5.396	9.64	Braatz96
16	IC 342	X–21	0.0001	034648.48	+680546.9	10.764	0.043	9.783	0.045	9.195	0.030	F03419+6756	3.654	19.24	132.8	132.8	Tarchi02a
17	UGC 3255	S2	0.0190	050950.18	+072900.0	12.758	0.028	12.034	0.035	11.691	0.034	F05071+0725	/	/	1.139	/	Braatz04
18	Mrk 3	S2,C	0.0134	061536.41	+710214.9	11.979	0.087	11.004	0.066	10.646	0.055	F06098+7103	0.713	2.896	3.770	3.36	Braatz04
19	NGC 2146	SBG	0.0029	061837.79	+782124.6	11.095	/	10.284	0.062	9.122	0.029	F06107+7822	6.228	17.58	131.0	184.0	Tarchi02b
20	VII Zw 073	S2	0.0405	063025.52	+634041.3	13.789	0.054	13.003	0.060	12.565	0.044	06256+6342	/	0.503	1.757	2.42	Kondratko06
21	NGC 2273	S2,C	0.0062	065008.65	+605044.8	11.954	0.073	11.077	0.075	10.579	0.045	F06456+6054	0.400	1.362	6.021	10.0	Zhang06,#
22	Mrk 78	S2	0.0373	074241.73	+651037.4	12.696	0.026	12.081	0.040	11.737	0.034	F07379+6517	0.128	0.555	1.110	1.13	Braatz04
23	Mrk 1210	S2,C?	0.0135	080405.85	+050649.8	13.261	0.080	12.531	0.102	11.748	0.050	F08014+0515	0.497	2.075	1.892	1.30	Braatz94, Braatz96
24	J0804+3607	Q2	0.6580	/	/	/	/	/	/	/	/	/	/	/	/	/	Barvainis05
25	0836+3327	/	0.0494	083622.80	+332738.7	14.174	0.034	13.509	0.035	13.129	0.036	/	/	/	/	/	Kondratko03
26	NGC 2639	LINER	0.0109	084338.06	+501220.1	12.022	0.070	10.990	0.064	10.629	0.044	F08400+5023	0.162	0.209	1.988	7.06	Braatz94, Braatz96
27	NGC 2782	SBG,C	0.0085	091405.12	+400649.3	11.701	0.025	10.822	0.021	10.554	0.023	F09109+4019	0.494	1.414	8.668	14.6	Braatz04
28	NGC 2824	S2	0.0092	091902.24	+261612.1	12.298	0.049	11.602	0.061	11.115	0.034	F09161+2628	/	/	1.026	1.89	Greenhill03
29	0927+493	LINER*	0.0341	093106.78	+490447.0	13.626	0.054	12.956	0.077	12.450	0.053	F09277+4917	0.140	4.494	1.662	2.30	Kondratko03
30	UGC 5101	ULIRG	0.0396	093551.60	+612111.7	13.492	0.066	12.260	0.053	11.231	0.034	09320+6134	0.253	1.045	12.09	20.2	Zhang06
31	Mrk 1419	LINER	0.0164	094036.39	+033437.1	12.451	0.062	11.831	0.086	11.313	0.050	09380+0348	/	/	0.769	1.66	Henkel02
32	NGC 2979	S2	0.0090	094308.66	–102259.9	13.051	0.097	12.279	0.083	11.825	0.075	F09406–1009	0.114	0.235	1.449	3.59	Greenhill03
33	NGC 3034	SBG	0.0146	095552.17	+694047.6	9.621	/	9.114	0.121	8.170	0.089	09517+6954	53.17	274.3	1170	1150	Claussen84,#
34	NGC 3079	S2/LINER,C	0.0038	100157.85	+554047.6	11.915	0.059	10.586	0.063	9.645	0.033	F09585+5555	1.523	2.272	44.50	89.2	Henkel84
35	IC 2560	S2	0.0097	101618.69	–333349.6	12.496	0.066	11.812	0.099	11.277	0.058	F10140–3318	0.296	0.944	3.244	6.11	Braatz96
36	Mrk 34	S2	0.0512	103408.54	+600152.1	14.094	0.095	13.280	0.087	12.652	0.045	F10308+6017	0.068	0.464	0.809	0.796	Henkel05
37	NGC 3393	S2,C	0.0124	104823.46	–250943.4	12.444	0.087	11.703	0.091	11.408	0.086	F10459–2453	0.131	0.753	2.251	3.87	Kondratko06; Zhang06
38	NGC 3556	X–35	0.0023	111130.91	+554027.6	13.578	0.129	12.864	0.132	12.475	0.137	F11085+5556	0.908	2.189	2.620	62.0	Henkel05,#
39	Arp 299	SBG,C	0.0010	112833.08	+583358.3	15.201	0.119	13.390	/	13.084	/	F11257+5850	3.805	23.19	103.7	107.0	Henkel05
40	NGC 3735	S2	0.0090	113557.24	+703207.8	12.475	0.089	11.616	0.090	11.350	0.089	F11330+7048	0.655	1.030	6.697	18.4	Greenhill97
41	NGC 4051	S/1.5	0.0023	120309.60	+443152.7	11.645	0.056	10.810	0.062	10.018	0.038	F12006+4448	0.855	1.590	7.131	23.9	Hagiwara03,#
42	NGC 4151	S1.5	0.0033	121032.58	+392421.1	10.262	0.026	9.436	0.025	8.519	0.020	/	/	/	/	/	Braatz04
43	NGC 4258	S1.9	0.0015	121857.50	+471814.3	11.069	0.086	10.542	0.114	10.068	0.077	12164+4735B	0.393	0.540	0.122	40.8	Claussen84, Braatz96
44	NGC 4293	LINER	0.0029	122112.83	+182257.3	12.583	0.067	11.853	0.067	11.289	0.049	F12186+1839	0.181	0.505	4.581	10.4	Kondratko06,#
45	NGC 4388	S2	0.0084	122546.77	+123943.2	12.482	0.066	11.730	0.091	11.066	0.051	F12232+1256	0.996	3.463	10.24	18.1	Braatz04
46	ESO 269–G012	S2	0.0163	125640.50	–465534.3	12.943	0.064	12.298	0.065	11.918	0.064	/	/	/	/	/	Greenhill03
47	NGC 4922	S2	0.0235	130125.26	+291849.6	14.009	0.071	13.231	0.075	12.504	0.056	F12590+2934	0.233	1.288	5.726	7.54	Braatz04
48	NGC 4945	S2,C	0.0019	/	/	/	/	/	/	/	/	13025–4911	3.627	14.24	388.1	620.0	dosSantos79,Braatz96
49	M51	S2,C	0.0020	132952.71	+471142.7	11.295	0.054	10.469	0.047	10.157	0.039	F13277+4727	1.801	2.611	32.68	138.0	Ho87,#
50	NGC 5256	S2	0.0270	133817.23	+481632.0	13.020	0.040	12.553	0.075	11.771	0.040	F13362+4831	2.307	0.977	7.342	11.1	Braatz04
51	NGC 5347	S2,C	0.0078	135317.81	+332926.9	12.809	0.030	12.145	0.028	11.572	0.026	13510+3344	0.289	0.922	1.443	2.64	Braatz96
52	NGC 5495	S2	0.0225	141223.35	–270629.1	13.759	0.098	13.037	0.136	12.675	0.098	F14095–2652	0.112	/	1.487	3.53	Kondratko03, 06
53	Circinus	S2,C	0.0014	141309.86	–652020.4	10.914	0.022	9.473	0.021	8.365	0.072	14092–6506	18.80	68.44	248.7	316.0	Gardner82,Braatz96
54	NGC 5506	S1?	0.0061	141314.88	–031227.7	12.072	0.050	10.434	0.044	9.037	0.024	F14106–0258	1.282	3.638	8.409	8.89	Braatz94, Braatz96
55	NGC 5643	S2,C	0.0039	143240.70	–441028.0	12.062	0.082	11.251	0.092	10.807	0.061	F14294–4357	1.098	3.647	19.49	38.2	Greenhill03
56	NGC 5728	S2	0.0095	144223.90	–171510.8	12.423	0.126	11.665	0.142	11.125	0.104	F14396–1702	0.243	0.882	8.163	14.7	Braatz04
57	UGC 9618B	S*	0.0339	145700.70	+243702.9	13.154	0.045	11.957	0.040	11.251	0.041	F14547+2449	0.221	0.434	5.988	15.6	Kondratko03
58	NGC 5793	S2	0.0115	145924.75	–164136.4	12.499	0.092	11.500	0.118	10.676	0.065	F14565–1629	0.190	/	6.208	8.96	Hagiwara97
59	NGC 6240	ULIRG,C	0.0243	165258.89	+022403.6	11.941	0.033	11.202	0.057	10.572	0.046	F16504+0228	0.558	3.417	22.68	27.8	Henkel84, Hagiwara02
60	NGC 6264	S2*	0.0339	165716.12	+275058.7	14.241	0.054	13.489	0.063	13.299	0.074	/	/	/	/	/	Kondratko03
61	NGC 6323	S2	0.0259	171318.03	+434656.6	13.127	/	12.830	0.061	12.590	0.061	F17118+4350	/	0.087	0.291	0.897	Braatz04
62	NGC 6300	S2,C?	0.0037	171659.54	–624913.9	11.428	0.024	10.579	0.025	10.103	0.026	F17123–6245	0.927	2.272	14.65	36.0	Greenhill03,#
63	ESO 103–G35	S2	0.0132	183820.31	–652539.2	13.015	0.071	12.118	0.083	11.510	0.047	F18333–6528	0.612	2.363	2.314	1.05	Braatz96
64	1937-0131	S2	0.0190	193938.92	–012433.3	14.071	0.068	12.998	0.056	12.464	0.045	F19370–0131	/	0.573	2.460	2.75	Greenhill03
65	3C403	FRII	0.0590	195215.79	+023024.3	14.210	0.093	13.371	0.102	12.705	0.066	F19497+0222	0.117	0.231	0.452	/	Tarchi03
66	NGC 6926	S2	0.0198	203306.11	–020138.5	14.156	0.117	13.322	0.152	12.775	0.095	F20304–0211	0.359	0.512	5.586	14.3	Greenhill03
67	NGC 6946	/	0.0002	203452.31	+600913.9	11.539	0.084	10.784	0.117	10.046	0.070	20338+5958	2.162	6.524	52.43	160.0	Claussen84
68	2158–380	S2	0.0332	220117.06	–374624.0	13.296	0.065	12.598	0.064	12.118	0.055	F21583–3800	/	0.140	0.349	0.532	Kondratko06
69	TXS 2226–18	LINER	0.0250	222912.50	–181047.2	14.964	0.082	14.237	0.101	13.844	0.080	F22265–1826	/	/	0.309	/	Koekemoer95: Giga
70	IC 1481	LINER	0.0203	231925.09	+055421.9	13.395	0.090	12.740	0.115	12.169	0.060	F23168+0537	/	0.275	1.410	1.51	Braatz96

(5) and (6), R.A. and Dec. (epoch 2000) in the 2MASS PSC; (7) and (8), J magnitude and uncertainty measured from the 2MASS PSC; (9) and (10), H magnitude and uncertainty measured from the 2MASS PSC; (11) and (12), K magnitude and uncertainty measured from the 2MASS (A blank in the columns (8), (10) and (12), means that the magnitude is only the upper-limited value (2MASS PSC), which will not be used in the following discussion); (13) IRASPSC/FSC name; (14) to (17) flux density at 12, 25, 60 and 100 μm in Jy from the IRAS PSC/FSC (only good quality flux densities are shown); (18) note. In the note the original references for each source from the Braatz Catalog are shown (see the References in detail). The symbol "#" indicates the kilo-maser from the Braatz Catalog.

In Table 1, (a) The type of nuclear activity is shown in the column (3) as: SBG, Starburst galaxy; S1, Seyfert 1; S2, Seyfert 2; LINER, Low-ionization nuclear emission line region; FRII, Fanarov-Riley type II gaxy; ULIRG, Ultraluminous infrared galaxy; C, Compton-thick; X-, the X-ray source in the absence of a starbust and a prominent nuclear source. The types are either from the Braatz Catalog or from Zhang et al. (2006) as well as from the Simbad database. The symbol "*" indicates the type from the Simbad database. (b) In the column (18) the symbol "#" indicates the kilo-maser from the Braatz Catalog. (c) The original reference can be seen in detail in the References.

2.3 Reddening Correction in Our Galaxy

For the 2MASS observations interstellar extinction correction should be made before using the data. For the interstellar extinction in our Galaxy, the $E(B-V)$ and interstellar extinction coefficient Av were obtained from the new maps given by Schlegel et al. (1998). In practice, Av was obtained through the NASA/IPAC Extragalactic Database (NED, 2004) for all the sources in Table 1. Then from Schlegel et al. (1998) A_J=0.272 Av, A_H=0.173 Av and A_K=0.110 Av can be obtained. Actually, in areas with $|b| \geq 30^{\circ}$, $E(B-V)$ is usually quite small, and as shown above, the interstellar extinction coefficients in the JHK bands are just about 1/4 to 1/10 of that of A_v. In addition, if the uncertainties of the measured magnitudes given in the 2MASS PSC are taken into account, most of the sources with $|b| \geq 30^{\circ}$ will have the interstellar extinction coefficients in the JHK bands smaller than the uncertainties of the measured magnitudes. Therefore, the interstellar extinction corrections were made for only 18 sources in Table 1. In the following discussion the magnitudes used in the JHK bands are all corrected for the interstellar extinctions according to the methods mentioned above.

3 COMPARISON BETWEEN SOURCES WITH AND WITHOUT DETECTED H_2O MASERS IN THE INFRARED

As mentioned in Section 1, in all the extragalactic H_2O maser surveys the detection rate has been rather low: only 70 out of about 1000 surveyed (Henkel et al. 2005; Lo 2005). However, a more detailed analysis is called for here. From Table 1 it is seen that all the H_2O maser galaxies are nearby sources with redshifts less than 0.06, except just one, J0804+3607 which has a redshift of 0.658. Henkel et al. (2005) and Lo (2005) pointed out that the main reason for the low detection rate is the limited sensitivities of the surveys, rather than an intrinsic lack of extragalactic H_2O masers. Now Braatz's web site gives a table listing all the sources surveyed before March 2002 by telescopes other than the 100 m Green Bank Telescope (GBT), West Virginia, USA (Lo 2005). This table lists about 900 sources, of which about 200 have redshifts greater than 0.06. In contrast, among the 70 detected sources shown in Table 1, only one source, J0804+3607, has a redshift of 0.658 and all the other sources have redshifts from 0.0001 to 0.06. This indicates that for the sources with Z >0.06 the detection rate is indeed very low at less than about 1/200 and the telescopes are not sensitive enough to sources at large distances. On the other hand, about 700 sources with Z <0.06 were still undetected. It means that for sources with Z <0.06 the detection rate should be about 10%.

Comparison between the H_2O maser detected sources and the non-detected sources at same distance scale in the infrared may be interesting for our understanding of the properties of extragalactic H_2O masers. The Braatz web site has also a catalog containing 134 non-detection sources from the GBT. The redshift range for those sources (always less than 0.06) are all compatible with the redshift range for the sources in Table 1. In order to compare infrared properties between the H_2O maser sources and non-detected sources, the non-detected source samples from the GBT are collected in Table 2. Similar to Section 2, the 2MASS and the IRAS counterparts of those sources are identified and the relevant information from the 2MASS PSC, the IRAS PSC/FSC and the Simbad database are shown in Table 2. Also corrections for interstellar

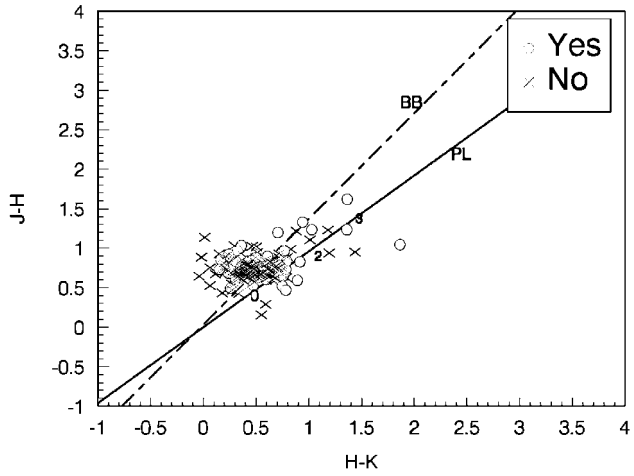

Fig. 1 2MASS $(J-H)$–$(H-K)$ diagram for the H_2O maser detected sources (Yes) and non-detected sources (No). The blackbody line and a power law curve with the spectral indices of 0, 2 and 3 are also plotted with the dashed line and the solid line respectively.

extinction in our Galaxy are made for the sources in Table 2 at the 2MASS bands. In the following discussion the 2MASS data referred to are all corrected for the interstellar extinction.

It is found from Tables 1 and 2 that 63 H_2O maser detected sources and 128 non-detected sources from the GBT have good quality JHK magnitudes. After correction for the interstellar extinction, the $(J-H)$–$(H-K)$ diagrams for the (H_2O maser) detected sources and the non-detected sources are plotted. See Figure 1. A blackbody line and a power law ($F=\nu^{\alpha}$) curve with spectral indices 0, 2 and 3 are also added. From Figure 1 it can be seen: (1) that some sources are very close to, or to the right of the power law curve, implying the power law radiation mechanism for such sources in the near infrared. However, more sources are close to or even to the left side of the blackbody line. For these sources, the origin of the radiation in the near infrared may not be described by the power law radiation, rather, thermal emission from starbursts may predominate (Chen et al. 2006); (2) For the 63 H_2O maser detected sources, the average near infrared colors are $\langle H-K\rangle$=0.54±0.06 and $\langle J-H\rangle$=0.77±0.04, while for the 128 non-detected sources, $\langle H-K\rangle$=0.48±0.06 and $\langle J-H\rangle$=0.74±0.03. These results show that the color distributions in the near infrared are quite similar for the two kinds of sources. Furthermore, a Kolmogorov-Smirnov test (hereafter K–S test) applied to the two distributions resulted in a K–S test probability = 0.002 with a correlation coefficient r=0.90, which confirms the similarity in the near infrared color distribution between the detected and the non-detected sources. This result implies that for both types, all the observed near infrared radiation is mainly from starlight in the the galaxy disk, not related to the production of the H_2O masers.

Tables 1 and 2 show that 50 H_2O maser detected sources and 58 non-detected sources have good quality flux densities at the IRAS 12, 25 and 60 μm, and that 54 H_2O maser detected sources and 73 non-detected sources have good quality flux densities at the IRAS 25, 60 and 100 μm. According to the equations given in the IRAS ES:

$$[12]-[25]=1.56-2.5\log(F_{12}/F_{25})\,, \tag{1}$$

$$[25]-[60]=1.88-2.5\log(F_{25}/F_{60})\,, \tag{2}$$

$$[60]-[100]=1.11-2.5\log(F_{60}/F_{100})\,, \tag{3}$$

the [12]-[25], [25]-[60] and [60]-[100] colors can be calculated. Thus we have the IRAS ([12]-[25])–([25]-[60]) and ([25]-[60])–([60]-[100]) diagrams shown in Figures 2 and 3, for both H_2O maser detected sources and non-detected sources. Again, a blackbody line and a power law curve are added to the figures.

Table 2 H_2O Maser Non-detected Sources Listed in the GBT

Name	Redshift	RA (2MASS 2000)	Dec	J	e_J	H	e_H	K	e_K	IRAS Name	F_{12}	F_{25}	F_{60}	F_{100}
UGC 1395	0.0172	015522.02	+063642.4	13.826	0.070	12.990	0.085	12.331	0.052	F01527+0622	/	/	0.467	1.20
0253–1641	0.0318	025602.65	–162915.6	13.649	0.054	12.937	0.055	12.288	0.046	F02536–1641	/	0.269	0.670	0.785
0258–1136	0.0299	030030.65	–112456.8	13.682	0.077	12.949	0.069	12.434	0.057	F02581–1136	0.200	0.476	0.508	/
0335+09	0.0350	033840.55	+095812.0	13.302	0.041	12.639	0.063	12.351	0.053	/	/	/	/	/
0354–1855	0.0253	035710.29	–184639.5	13.603	0.120	12.786	0.119	12.349	0.113	F03549–1855	0.130	0.106	1.03	3.25
0414+00	0.0336	041643.13	+001622.1	15.407	0.148	14.731	0.181	14.139	0.128	F04141+0008	0.083	0.208	1.80	2.79
0445–1741	0.0301	044730.67	–173548.6	13.405	0.082	12.738	0.110	12.193	0.069	/	/	/	/	/
0446–2349	0.0271	044855.95	–234347.6	13.639	0.083	12.875	0.082	12.415	0.074	/	/	/	/	/
07570+2334	0.0292	080004.02	+232616.4	13.704	0.071	13.135	0.080	12.653	0.063	/	/	/	/	/
UGC 4332	0.0183	081937.80	+210652.1	13.492	0.071	12.467	0.076	12.002	0.065	F08167+2116	/	0.231	0.807	2.09
0942+09	0.0132	094529.36	+093610.4	14.242	0.097	13.592	0.118	13.175	0.082	/	/	/	/	/
1034+060	0.0118	103635.78	+055438.1	13.808	0.096	13.118	0.115	12.560	0.068	F10340+0609	/	/	0.389	/
1116–2909	0.0303	111853.45	–292527.5	13.662	0.087	12.996	0.116	12.322	0.065	F11164–2908	/	0.164	1.26	3.29
1258–3208	0.0314	130120.38	–322410.4	14.005	0.095	13.272	0.124	12.823	0.079	F12585–3208	/	/	0.592	1.67
TXS1319–164	0.0171	132224.47	–164342.4	12.341	0.078	11.568	0.094	10.877	0.050	F13197–1627	0.878	2.86	5.89	5.48
1322+2918	0.0234	132442.60	+290258.9	15.397	0.123	15.105	0.182	14.515	0.135	/	/	/	/	/
UGC 8621	0.0200	133739.91	+390916.4	13.939	0.083	12.534	/	12.141	/	F13354+3924	0.122	0.147	0.965	2.47
1431–3237	0.0254	143445.47	–325032.6	13.979	0.062	13.327	0.089	12.852	0.060	F14317–3237	/	0.262	0.826	/
Ark 479	0.0198	153552.49	+143103.7	13.967	0.070	13.293	0.110	12.871	0.068	F15335+1440	/	/	0.261	/
1548–0344	0.0301	155041.50	–035318.0	13.470	0.068	12.674	0.073	11.978	0.054	F15480–0344	0.185	0.729	1.07	/
2319+09	0.0395	232200.67	+091748.1	14.230	0.072	13.619	0.080	12.921	0.060	F23194+0901	/	0.257	1.39	2.14
3C 317	0.0344	151644.49	+070117.7	14.343	0.129	13.560	0.142	13.035	0.112	/	/	/	/	/
Ark 539	0.0164	182848.08	+502220.9	13.372	0.046	12.500	0.039	12.311	0.035	/	/	/	/	/
Fair 1140	0.0373	063757.12	–325240.9	14.147	0.071	13.483	0.088	12.988	0.060	/	/	/	/	/
Fair 1149	0.0283	101319.91	–355857.7	13.770	0.083	12.946	0.097	12.517	0.065	F10111–3544	/	0.211	/	/
IC 614	0.0345	102651.85	–032753.1	14.133	0.078	13.523	0.098	13.074	0.071	/	/	/	/	/
IC 694	0.0101	112827.26	+583442.2	15.588	0.087	14.942	0.131	14.983	0.151	/	/	/	/	/
IC 4553	0.0181	153457.24	+233011.4	13.579	0.146	12.363	0.110	11.484	0.069	F15327+2340	0.484	7.91	104.0	112.0
III Zw 101	0.0383	231721.14	+180321.3	14.303	0.073	13.634	0.088	13.277	0.071	/	/	/	/	/
Mrk 176a	0.0278	113235.35	+525650.2	14.485	0.076	13.815	0.096	13.259	0.066	/	/	/	/	/
Mrk 176b	0.0278	113236.74	+525651.8	13.581	0.056	12.989	0.070	12.613	0.058	11298+5313	/	0.180	0.689	/
Mrk 176c	0.0278	113240.23	+525701.3	12.871	0.044	12.245	0.057	11.459	0.039	F11299+5313	0.170	0.242	0.694	1.51
Mrk 198	0.0246	120914.13	+470330.1	12.879	0.032	12.335	0.047	12.032	0.040	F12067+4720	/	0.136	0.624	0.863
Mrk 273	0.0372	134442.08	+555313.0	13.392	0.077	12.511	0.074	11.793	0.048	F13428+5608	0.235	2.28	21.7	21.4
Mrk 298	0.0342	160536.80	+174807.5	13.249	0.034	12.522	0.039	12.132	0.041	/	/	/	/	/
Mrk 334	0.0220	000309.60	+215736.8	12.912	0.055	11.925	0.053	11.096	0.033	F00006+2141	0.226	1.05	4.34	4.32
Mrk 359	0.0167	012732.52	+191043.8	12.657	0.040	12.043	0.063	11.360	0.038	F01248+1855	0.119	0.438	1.13	1.74
Mrk 372	0.0309	024920.68	+191814.4	13.176	0.052	12.383	0.050	11.823	0.038	F02465+1905	/	0.168	0.303	1.87
Mrk 403	0.0242	094044.52	+211403.3	13.921	0.053	13.377	0.069	13.107	0.072	/	/	/	/	/
Mrk 423	0.0322	112648.51	+351503.2	13.060	0.038	12.363	0.046	11.915	0.038	F11241+3531	/	0.181	1.42	2.39
Mrk 461	0.0162	134717.75	+340855.8	13.181	0.042	12.558	0.050	12.209	0.047	/	/	/	/	/
Mrk 477	0.0380	144038.10	+533016.0	14.006	0.047	13.270	0.057	12.651	0.047	F14390+5343	0.126	0.509	1.31	1.85
Mrk 516	0.0286	215622.26	+072200.3	13.432	0.058	12.771	0.067	12.145	0.052	F21538+0707	/	0.231	1.33	2.32
Mrk 573	0.0173	014357.77	+022059.5	12.832	0.077	12.023	0.085	11.453	0.051	01413+0205	/	0.798	1.27	1.26
Mrk 612	0.0205	033040.88	–030815.8	13.099	0.070	12.466	0.081	11.913	0.052	F03281–0318	0.128	0.268	1.16	1.81
Mrk 622	0.0232	080741.00	+390015.2	13.188	0.042	12.507	0.051	11.980	0.031	F08043+3909	/	0.405	1.28	1.43
Mrk 745	0.0107	113956.30	+165718.0	14.064	0.040	13.629	0.061	13.449	0.062	/	/	/	/	/
Mrk 883	0.0376	162952.87	+242638.1	13.333	0.031	12.589	0.036	12.223	0.033	F16277+2433	/	0.217	1.02	1.14
Mrk 917	0.0245	224107.59	+321011.1	12.957	0.052	12.142	0.064	11.347	0.027	F22388+3154	0.186	0.609	3.71	5.95
Mrk 937	0.0297	001009.98	–044237.8	14.104	0.089	13.307	0.080	12.876	0.077	F00076–0459	/	/	0.524	1.25
Mrk 955	0.0349	003735.81	+001650.6	13.386	0.079	12.694	0.099	12.291	0.076	F00350+0000	/	/	0.938	1.78
Mrk 1058	0.0173	024951.81	+345916.8	13.253	0.054	12.449	0.053	11.982	0.040	F02467+3446	/	0.171	0.587	1.39
Mrk 1073	0.0233	031501.43	+420208.9	12.594	0.030	11.698	0.034	11.397	0.033	F03117+4151	0.443	1.41	8.17	11.1
Mrk 1098	0.0350	152940.58	+302909.3	13.208	0.026	12.477	0.024	11.819	0.025	F15276+3039	/	0.10	0.338	0.566
Mrk 1239	0.0190	095219.10	–013643.6	12.188	0.036	10.938	0.040	9.721	0.026	F09497–0122	0.650	1.14	1.34	2.41
Mrk 1388	0.0212	145037.85	+224403.4	13.803	0.048	12.979	0.047	12.230	0.034	F14483+2256	/	0.231	0.174	0.571
NGC 334	0.0307	005849.83	–350657.6	14.077	0.097	13.296	0.116	12.889	0.086	F00564–3523	/	/	0.657	1.76
NGC 404	0.0001	010927.00	+354304.8	11.457	0.038	10.562	0.032	10.547	0.038	F01066+3527	/	0.204	2.14	3.98
NGC 600	0.0062	013305.30	–071841.3	14.470	/	14.813	0.139	13.573	/	F01305–0734	/	/	0.562	2.57
NGC 788	0.0136	020106.46	–064857.1	12.860	0.109	12.032	0.125	11.394	0.063	F01586–0703	0.187	/	0.5111	0.593
NGC 1144	0.0288	025512.22	–001100.8	13.166	0.101	12.424	0.151	11.730	0.077	F02526–0023	0.278	0.633	5.30	11.3
NGC 1167	0.0164	030142.34	+351220.2	12.403	0.063	11.668	0.062	11.232	0.050	/	/	/	/	/
NGC 1229	0.0363	030810.84	–225736.7	14.202	0.089	13.344	0.099	12.747	0.060	F03059–2309	0.147	0.631	1.55	2.06
NGC 1358	0.0134	033339.69	–050522.1	12.426	0.091	11.832	0.107	11.363	0.090	F03311–0515	/	/	0.378	0.925
NGC 1365	0.0055	033336.38	–360825.7	11.344	0.091	10.240	0.097	9.229	0.047	F03316–3618	3.37	10.8	76.1	142.0
NGC 1409	0.0250	034110.46	–011809.6	13.010	0.089	12.252	0.099	11.720	0.071	F03386–0127	/	0.186	0.867	2.18
NGC 1410	0.0253	034110.72	–011755.7	13.651	0.087	12.823	0.086	12.345	0.060	F03386–0127	/	0.186	0.867	2.18
NGC 1667	0.0152	044837.17	–061911.9	12.395	0.062	11.638	0.064	11.248	0.063	F04461–0624	0.429	0.677	5.95	1.47
NGC 1685	0.0140	045234.30	–025657.3	13.812	0.077	13.078	0.093	12.548	0.058	F04500–0301	/	0.218	0.976	1.53
NGC 2110	0.0076	055211.38	–072722.5	11.930	0.104	11.066	0.113	10.149	0.058	F05497–0728	0.349	0.840	4.13	5.68
NGC 2273	0.0062	065008.65	+605044.8	11.954	0.073	11.077	0.075	10.579	0.045	F06456+6054	0.400	1.36	6.02	10.0
NGC 2377	0.0082	072456.82	–093933.2	13.173	0.085	12.286	0.092	11.763	0.069	07225–0933	0.418	0.948	8.93	17.9
NGC 2768	0.0046	091137.41	+600215.1	11.313	0.057	10.427	0.051	10.447	0.055	F09077+6014	0.090	/	0.369	1.16
NGC 2841	0.0021	092202.69	+505835.6	10.731	0.065	10.000	0.078	9.806	0.075	F09186+5111	0.282	0.218	3.03	18.8
NGC 2911	0.0106	093346.10	+100909.0	12.331	0.087	11.518	0.106	10.903	0.055	F09311+1022	/	/	0.219	/
NGC 2992	0.0077	094541.94	–141934.8	12.095	0.093	11.209	0.113	10.412	0.054	09432–1405	0.594	1.37	6.87	14.4

Table 2 —*Continued.*

Name	Redshift	RA (2MASS 2000)	Dec	J	e_J	H	e_H	K	e_K	IRAS Name	F_{12}	F_{25}	F_{60}	F_{100}
NGC 3010b	0.0153	095033.15	+441851.6	13.078	0.031	12.426	0.036	12.077	0.031	/	/	/	/	/
NGC 3031	0.0001	095533.16	+690355.1	9.642	0.080	8.961	0.112	8.434	0.071	F09514+6918	0.746	0.785	6.81	32.0
NGC 3185	0.0041	101738.56	+214117.6	12.648	0.044	11.906	0.045	11.589	0.038	F10148+2156	0.155	0.140	1.43	3.67
NGC 3227	0.0038	102330.57	+195154.3	11.265	0.036	10.528	0.043	9.923	0.027	F10207+2007	0.667	1.76	7.82	17.6
NGC 3362	0.0278	104451.74	+063548.7	14.455	0.136	13.693	0.129	13.244	0.119	/	/	/	/	/
NGC 3561	0.0287	111113.19	+284147.1	13.060	0.039	12.255	0.037	11.827	0.034	/	/	/	/	/
NGC 3642	0.0053	112217.88	+590428.3	12.807	0.100	12.182	0.106	11.864	0.078	F11193+5921	0.127	0.0990	1.44	4.58
NGC 3660	0.0123	112332.27	–083930.7	13.596	0.096	12.940	0.104	12.527	0.083	F11210-0823	0.193	0.224	1.87	4.54
NGC 3898	0.0039	114915.28	+560504.5	11.144	0.065	10.406	0.075	9.928	0.049	F11465+5621	0.108	/	0.415	2.02
NGC 3921	0.0197	115106.86	+550443.4	12.113	0.031	11.425	0.035	11.060	0.029	F11484+5521	/	0.108	0.828	/
NGC 3982	0.0035	115628.12	+550731.0	12.721	0.064	12.253	0.084	11.978	0.080	F11538+5524	0.507	0.834	6.57	15.2
NGC 3998	0.0036	115756.13	+552712.8	10.277	0.044	9.602	0.055	9.344	0.051	F11553+5543	0.138	0.159	0.438	0.934
NGC 4013	0.0027	115831.31	+435648.7	13.410	0.128	11.381	/	10.861	/	F11559+4413	0.240	0.299	5.70	20.1
NGC 4036	0.0048	120126.74	+615344.7	10.907	0.041	9.880	0.031	9.583	0.030	F11589+6210	0.086	/	0.501	1.45
NGC 4074	0.0225	120429.66	+201858.5	13.052	0.054	12.125	0.056	11.406	0.038	/	/	/	/	/
NGC 4111	0.0026	120703.12	+430356.4	10.167	0.037	9.325	0.035	9.058	0.031	/	/	/	/	/
NGC 4117	0.0030	120746.14	+430734.9	12.764	0.041	12.094	0.048	11.816	0.039	/	/	/	/	/
NGC 4192	0.0005	121348.29	+145401.9	11.532	0.096	10.599	0.090	10.244	0.077	F12112+1510	0.355	0.440	5.92	19.7
NGC 4278	0.0021	122006.82	+291650.5	11.025	0.113	10.495	0.150	10.049	0.102	F12176+2933	/	/	0.557	1.57
NGC 4303	0.0052	122154.92	+042825.8	11.379	0.067	10.783	0.106	10.194	0.062	F12193+0445	1.06	1.40	23.6	64.7
NGC 4419	0.0009	122656.44	+150250.7	11.059	0.041	9.924	0.031	9.912	0.038	F12244+1519	0.539	1.44	7.99	16.9
NGC 4450	0.0064	122829.59	+170506.0	11.271	0.041	10.518	0.047	10.456	0.053	F12259+1721	0.108	0.130	1.34	6.95
NGC 4486	0.0042	123049.43	+122327.9	11.439	0.109	11.284	0.222	10.733	0.152	F12282+1240	0.231	/	0.394	/
NGC 4501	0.0076	123159.16	+142513.5	11.278	0.052	10.139	/	9.844	/	F12294+1441	1.02	1.28	13.7	54.7
NGC 4569	0.0040	123649.79	+130946.6	10.817	0.045	10.146	0.057	10.033	0.055	F12343+1326	0.479	1.05	7.56	23.7
NGC 4579	0.0050	123743.52	+114905.7	11.241	0.100	10.625	0.142	10.023	0.083	F12351+1205	0.349	0.379	4.74	18.1
NGC 4941	0.0037	130413.11	–053305.7	12.301	0.083	11.607	0.107	11.268	0.080	F13016–0517	0.184	0.527	1.38	4.19
NGC 5005	0.0032	131056.26	+370332.4	10.273	0.037	9.475	0.037	8.994	0.034	F13086+3719	0.951	1.21	19.6	54.3
NGC 5128	0.0018	132527.65	–430109.2	11.334	0.127	10.347	0.166	8.847	0.080	F13225–4245	13.3	17.3	162.0	314.0
NGC 5135	0.0137	132544.05	–295000.7	12.436	0.110	11.710	0.139	10.937	0.082	F13229–2934	0.638	2.40	16.9	28.6
NGC 5195	0.0016	132959.52	+471558.2	9.916	0.036	9.118	0.036	8.582	0.026	F13278+4731	0.721	1.45	10.4	/
NGC 5252	0.0222	133815.87	+043233.3	13.064	0.097	12.375	0.105	11.800	0.074	/	/	/	/	/
NGC 5283	0.0096	134105.74	+674019.9	11.954	0.023	11.264	0.028	11.051	0.028	/	/	/	/	/
NGC 5371	0.0086	135539.93	+402742.3	11.962	0.046	11.302	0.048	10.820	0.038	F13535+4042	0.207	0.223	3.31	14.8
NGC 5427	0.0087	140326.04	–060150.5	13.538	0.118	12.919	0.168	12.235	0.079	14008–0547	0.283	0.623	4.86	16.5
NGC 5635	0.0144	142831.76	+272432.4	12.444	0.069	11.668	0.080	11.082	0.045	F14263+2737	0.084	/	0.288	1.78
NGC 5674	0.0250	143352.28	+052730.1	13.032	0.069	12.237	0.085	11.577	0.051	F14313+0540	0.144	0.281	1.44	3.73
NGC 5675	0.0136	143239.85	+361808.0	12.389	0.047	11.731	0.061	11.119	0.041	F14306+3631	0.101	/	0.472	1.81
NGC 5695	0.0141	143722.15	+363404.3	12.642	0.044	11.976	0.050	11.622	0.042	F14353+3646	/	0.129	0.566	1.79
NGC 5851	0.0217	150653.40	+125131.5	14.019	0.077	12.788	/	12.954	0.063	F15044+1302	/	0.114	0.622	2.12
NGC 5899	0.0085	151503.27	+420259.6	12.473	0.065	11.456	0.049	10.954	0.038	F15132+4214	0.261	0.386	3.41	10.7
NGC 5929	0.0089	152606.17	+414014.4	12.650	0.048	11.800	0.042	11.433	0.034					
NGC 5953	0.0066	153432.38	+151137.8	11.844	0.062	11.191	0.091	10.703	0.055	F15322+1521	0.533	1.16	10.0	19.0
NGC 6211	0.0176	164127.66	+574701.0	12.361	0.044	11.660	0.049	11.340	0.037	/	/	/	/	/
NGC 6251	0.0239	163231.97	+823216.5	11.940	0.035	11.041	0.032	10.691	0.027	/	/	/	/	/
NGC 6500	0.0099	175559.78	+182017.6	11.779	0.033	10.821	0.027	10.622	0.031	F17537+1820	0.101	0.101	0.642	2.55
NGC 6764	0.0080	190816.38	+505559.4	12.512	0.029	11.763	0.035	11.506	0.035	F19070+5051	0.361	1.29	6.33	11.6
NGC 6951	0.0048	203714.07	+660620.2	11.872	0.099	10.838	0.086	10.405	0.057	F20366+6555	0.617	1.37	13.2	37.5
NGC 7212	0.0263	220701.99	+101400.9	13.351	0.079	12.697	0.102	12.250	0.071	F22045+0959	0.196	0.769	2.88	4.89
NGC 7217	0.0032	220752.39	+312133.6	11.620	0.078	10.674	0.071	10.115	0.035	F22056+3106	0.376	0.301	4.96	18.5
NGC 7450	0.0104	230047.81	–125506.7	12.570	0.036	11.854	0.038	11.449	0.035	/	/	/	/	/
NGC 7674	0.0290	232756.71	+084644.4	13.192	0.077	12.252	0.085	11.059	0.037	F23254+0830	0.672	1.90	5.59	8.15
NGC 7682	0.0171	232903.91	+033200.0	13.490	0.103	12.891	0.117	12.239	0.073	/	/	/	/	/
NGC 7743	0.0056	234421.15	+095602.9	11.604	0.033	11.154	0.052	10.780	0.043	F23417+0939	/	/	0.791	2.53
[SP] 55	0.0329	154744.14	+412408.3	13.902	0.041	13.282	0.050	12.937	0.046	F15460+4133	0.088	0.10	0.339	/
UGC 6100	0.0292	110133.97	+453914.1	13.341	0.048	12.585	0.052	12.387	0.054	F10587+4555	0.145	0.202	0.574	1.50
UGC 10567	0.0308	164909.60	+361325.7	13.432	0.055	12.787	0.067	12.396	0.056	/	/	/	/	/
UGC 12056	0.0250	222952.46	+364309.3	13.099	0.039	12.257	0.042	12.002	0.040	22276+3627	/	/	0.518	1.43

From Figure 2 it can be derived that the average values of the colors, $\langle$[12]–[25]$\rangle$= 2.80$\pm$0.06 and $\langle$[25]–[60]$\rangle$ = 3.55$\pm$0.07 for the H_2O maser detected sources while $\langle$[12]–[25]$\rangle$ = 2.31$\pm$0.05 and $\langle$[25]–[60]$\rangle$ = 3.77$\pm$0.06 for the non-detected sources. It is obvious that statistically quite similar distributions in the color [25]–[60] are found in the two groups of sources, while the [12]–[25] distributions are clearly different. The H_2O maser detected sources have redder colors and a steeper slope between 12 μm and 25 μm than the non-detected sources. Although this result confirms the general suggestion from Collison et al. (1995) and Lo (2005) that infrared radiations in the far infrared may play an important role for the large luminosity

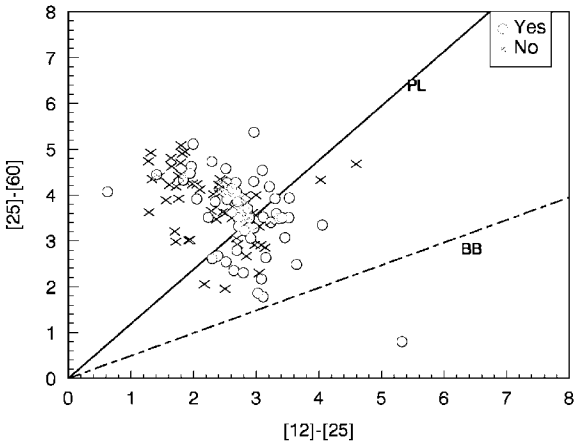

Fig. 2 IRAS ([12]-[25])–([25]-[60]) diagram for the H_2O maser detected sources (Yes) and non-detected sources (No). The blackbody line (BB) and the power law curve (PL) are also plotted with the dashed line and the solid line respectively.

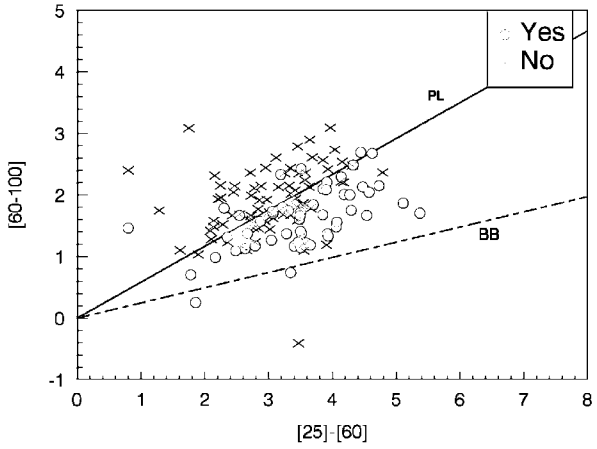

Fig. 3 IRAS ([25]-[60])–([60]-[100]) diagram for the H_2O maser detected sources (Yes) and non-detected sources (No). The blackbody line (BB) and the power law curve (PL) are also plotted with the dashed line and the solid line respectively.

observed in extragalactic H_2O masers, the result here indicates that the infrared radiation in 12–25 μm is important, but that in 25–60 μm may not be so important. In addition, it can be seen from Figure 2 that the majority of both categories of sources are close to, or to the left of the power law line, indicative of non-thermal radiation in this infrared region. Furthermore, it is obvious that the most striking result in Figure 2 is the confirmation of the anti-correlation between the colors [12]–[25] and [25]–[60], found by Henkel et al. (1986) and Greenhill et al. (2002) from quite a small sample, and this anti-correlation is present not only in the H_2O maser detected sources but also in the non-detected sources. According to Henkel et al. (1986), the anti-correlation is caused by the coexistence of lager and very small dust grains because the latter, when heated momentarily by single photon absorption are responsible for the bulk of the 12 μm radiation. It is not surprising that the non-detected sources also show this anti-correlation because most extragalactic H_2O

maser surveys are biased to Seyfert 2 and LINER galaxies (Lo 2005). If Seyfert 1 galaxies are largely included, then such an anti-correlation will not be present (Greenhill et al. 2002). Incidentally, this anti-correlation is also found for the interstellar H_2O masers in our Galaxy (Henkel 1986; Esimbek et al. 2005).

From Figure 3 it can be derived that the average values of the IRAS colors, $\langle$[25]–[60]$\rangle$ = 3.55$\pm$0.06 and $\langle$[60]–[100]$\rangle$ = 1.64$\pm$0.08 for the H_2O maser detected sources, while $\langle$[25]–[60]$\rangle$= 3.78$\pm$0.07 and $\langle$[60]–[100]$\rangle$= 1.92$\pm$0.07 for the non-detected sources. It is seen that similar distributions in [25]–[60] can be found for the two groups, as is shown in Figure 2, but the distributions in [60]–[100] for the two groups of sources are different. Statistically, the non-detected sources have redder 60–100 μm colors than the H_2O maser detected sources. In addition, Figure 3 shows that the majority of both categories are close to the power law line indicative of non-thermal radiation in this infrared region, and many of the non-detected sources are closer to, and even to the left side of the power law line. The distributions in Figures 2 and 3 seem to indicate that the infrared properties of both the H_2O maser detected sources and the non-detected sources of types Seyfert 2 and LINER are clearly influenced by the central AGNs. In contrast, in the same IRAS region the OH maser sources are closer to the blackbody line indicative of thermal radiation (Chen et al. 2007). One possible explanation may be the different distances from the central AGNs for H_2O maser sources and the OH maser sources. For most H_2O maser sources the distances are only about a few pc while for the OH maser sources they can be as much as 100 pc or thereabout (Lo 2005).

From the results above it may be suggested that the infrared properties of the H_2O maser detected sources and the non-detected sources are similar in the near infrared region and the IRAS 25–60 μm region, but different in the IRAS 12–25 μm region and in the IRAS 60–100 μm region. This implies that the sources with H_2O maser detection have probably redder colors and a steeper slope in 12–25 μm, but bluer colors and a flatter slope in the 60–100μm. The results for the present larger sample are in full agreement with the previous study based on a smaller sample (Braatz et al. 1997 had only about 20 sources) that the infrared properties at 12–25 μm and probably at 60–100 μm may be important for producing the H_2O masers.

4 INFRARED PROPERTIES OF THE H_2O MASER GALAXIES WITH DIFFERENT NUCLEAR ACTIVITY TYPES

For the galaxies with extragalactic H_2O masers (hereafter H_2O maser galaxies) the types of nuclear activities from the Braatz Catalog or from Zhang et al. (2006) as well as from the Simbad database are given in Table 1. The near infrared two-color diagram from the 2MASS observations is plotted in Figure 4 for the H_2O maser galaxies of different nuclear activity types. In addition, using Equations (1) to (3), [12]-[25],

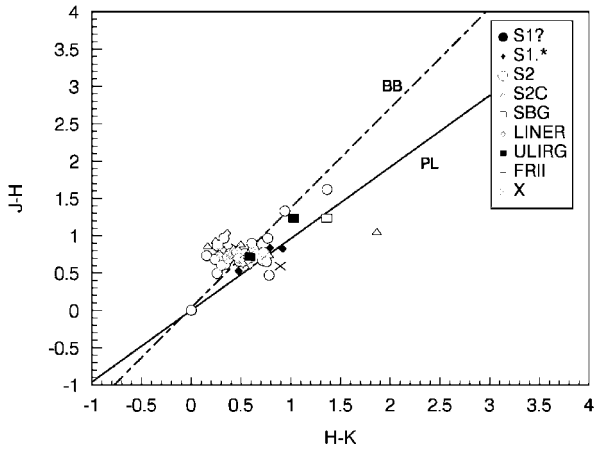

Fig. 4 2MASS $(J-H)$–$(H-K)$ diagram for the H_2O maser galaxies with different nuclear activity types. The meaning for the symbols can be found in Section 4. The blackbody line (BB) and the power law curve (PL) are also plotted with the dashed line and the solid line respectively.

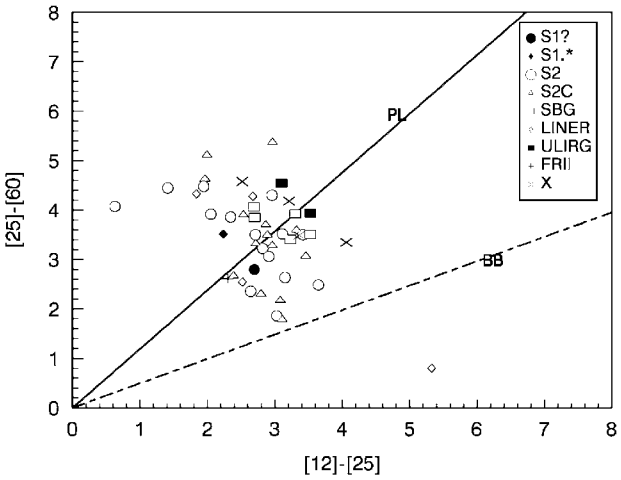

Fig. 5 IRAS ([12]-[25])–([25]-[60]) diagram for the H_2O maser galaxies with different nuclear activity types. The meaning for the symbols is as same as in Fig. 4. The blackbody line (BB) and the power law curve (PL) are also plotted with the dashed line and the solid line respectively.

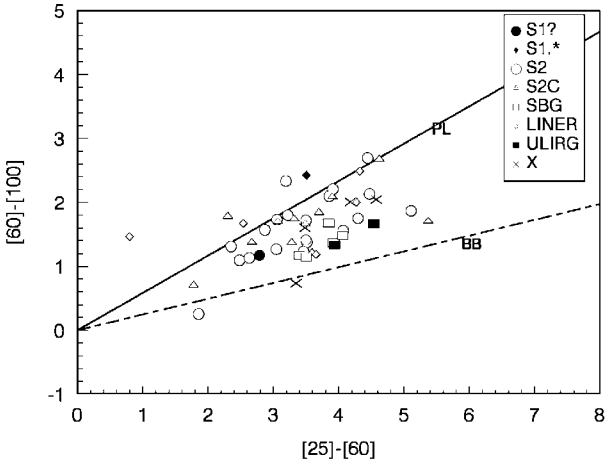

Fig. 6 IRAS ([25]-[60])–([60]-[100]) diagram for the H_2O maser galaxies with different nuclear activity types. The meaning for the symbols is as same as in Fig. 4. The blackbody line (BB) and the power law curve (PL) are also plotted with the dashed line and the solid line respectively.

[25]-[60] and [60]-[100] colors can be obtained, hence the IRAS ([12]-[25])–([25]-[60]) and ([25]-[60])–([60]-[100]) diagrams can be constructed. See Figures 5 and 6. The symbols used in those figures are: S1, Seyfert 1; S1.*, Seyfert 1.5 to Seyfert 1.9; S2: Seyfert 2; S2C, Compton-thick Seyfert 2; SBG, Starburst galaxy; LINER, Low-ionization nuclear emission line region; ULIRG, Ultraluminous infrared galaxy; FRII, Fanarov-Riley type II galaxy; X, the X-ray source . Note the blackbody line and the power law line are also shown in those figures.

It is seen from Figure 4 that the distributions of the H_2O maser galaxies of different nuclear activity types are not so different, indicating a similar environment mainly from starlight on the galaxy disks in the near infrared. Although in the region very close to the central engine there might be also strong near

infrared radiations, but those radiations are not easily detected, because for most H_2O maser galaxies the nuclear tori are viewed edge-on (e.g. Henkel et al. 2003; Lo 2005).

It can be seen from Figure 5 that, statistically, in the IRAS 12–60 μm region the X-ray sources, the SBG sources and the ULIRG sources have slightly redder colors than the other sources; the distributions of the Seyfert 2 sources and the Compton-thick Seyfert 2 sources are quite similar; some Seyfert 2 sources and the Compton-thick Seyfert 2 sources are close to the blackbody line indicative of the thermal radiation, and the FRII, Seyfert 1 and the Seyfert 1.5 to Seyfert 1.9 sources have rather bluer colors. These distributions are reasonable in the frame of the unified scheme for AGNs (Antonicci 1993; Ghisellini et al. 1993).

While, as mentioned above, different type sources have different distributions in the 25–60 μm region, Figure 6 shows their distributions in the IRAS 60–100 μm region are similar. This indicates a similar environment of very cold dust and gas in the galaxy disks.

5 SUMMARY

All galaxies with extragalactic H_2O maser sources so far observed are collected in this paper, to a total of 70 galaxies. Their infrared properties are studied using the 2MASS and the IRAS photometric data. Comparing the H_2O maser detected sources and non-detected sources in the infrared, it is found that the the IRAS 12–25 μm and 60–100 μm ranges may be important for producing H_2O masers in galaxies. It is also found that the H_2O maser galaxies with different nuclear activity types have rather different infrared properties mainly in the IRAS 12–60 μm region. The results may help us to understand the relation between the infrared environment and the H_2O masers produced in such galaxies.

Acknowledgements This publication makes use of data products from the Two Micron All Sky Survey (2MASS), which is a joint project of the University of Massachusetts and the Infrared Processing and Analysis Center, funded by the National Aeronautics and Space Administration and the National Science Foundation of the United States. We are grateful to the referee for his/her fruitful suggestions. This work is supported by the National Nature Science Foundation of China (Nos. 10533050 and 10503011) and the Chinese Academy of Sciences. This work has also made use of the NASA ADS database, the CDS Simbad and VizieR Databases and the NASA/IPAC Extragalactic Database (NED, *http://nedwww.ipac.caltech.edu/*).

References

Antonicci R., 1993, ARA&A, 31, 473
Barvainis R., Antonucci R., 2005, ApJ, 628, L89 (Barvainis05)
Braatz J. A., Wilson A. S., Henkel C., 1994, ApJ, 437, L99 (Braatz94)
Braatz J. A., Wilson A. S., Henkel C., 1996, ApJS, 106, 51 (Braatz96)
Braatz J. A., Wilson A. S., Henkel C., 1997, ApJS, 110, 321
Braatz J. A., Henkel C., Greenhill L. J. et al., 2004, ApJ, 617,L29 (Braatz04)
Chen P. S., Zhang P., 2007, AJ, 131, 1942
Chen P. S., Shan H. G., Gao Y. F., 2007, AJ, 133, 496
Churchwell E., Witzel A., Huchtmeier W. et al., 1977, A&A, 54, 969 (Churchwell77)
Claussen M. J., Heiligman G. M., Lo K. Y., 1984, Nature, 310, 298 (Claussen84)
Collison A. J., Watson W. D., 1995, ApJ, 452, L103
Dos Santos P. M., Lepine J. R. D., 1979, Nature, 278, 34 (dosSantos79)
Elitzur M., 1992, ARA&A, 30, 75
Esimbek J., Wu Y. F., Wang J. Z., 2005, Chin. J. Astron. Astrophys. (ChJAA), 6, 587
Falcke H., Henkel C., Peck A. B. et al., 2000, A&A, 358, L17 (Falcke00)
Gardner F. F., Whiteoak J. B., 1982, MNRAS, 201, 13P (Gardner82)
Ghisellini G., Padovani P., Celotti A. et al., 1993, ApJ, 407, 65
Greenhill L. J., Herrnstein J. R., Moran J. M. et al., 1997, ApJ, 486, L15 (Greenhill97)
Greenhill L. J., Ellingsen S. P., Norris R. P. et al., 2002, ApJ, 565, 836 (Greenhill02)
Greenhill L. J., Kondratko P. T., Lovell J. E. J. et al., 2003, ApJ, 582, L11 (Greenhill03)
Hagiwara Y., Kohno K., Kawabe R. et al., 1997, PASJ, 49, 171 (Hagiwara97)
Hagiwara Y., Diamond P. J., Miyoshi M., 2002, A&A, 383, 65 (Hagiwara02)

Hagiwara Y., Diamond P. J., Miyoshi M. et al., 2003, MNRAS, 344, L53 (Hagiwara03)
Henkel C., Guesten R., Downes D. et al., 1984, A&A, 141, L1 (Henkel84)
Henkel, C., Wouterloot, J.G.A., Bally, J., 1986, A&A, 155, 193 (Henkel86)
Henkel C., Braatz J. A., Greenhill L. J. et al., 2002, A&A, 394, L23 (Henkel02)
Henkel C., Braatz J. A., 2003, Acta Astronomica Sinica, 44 Suppl., 55
Henkel C., Braatz J. A., Tarchi A. et al., 2004, Ap&SS, 295, 107
Henkel C., Peck A. B., Tarchi A. et al., 2005, A&A, 436, 75 (Henkel05)
Ho P. T. P., Martin R. N., Henkel C. et al., 1987, ApJ, 320, 663 (Ho87)
Huchtmeier W. K., Witzel A., Kuehr H. et al., 1978, A&A, 64, L21 (Huchtmeier78)
IRAS Explanatory Supplement, 1988, GPO, Washington, DC (IRAS ES)
Koekemoer A. M., Henkel C., Greenhill L. J. et al., 1995, Nature, 378, 697 (Koekemoer95)
Kondratko P. T., Greenhill L. J., Moran J. M. et al., 2003, BAAS, 35, 1311 (Kondratko03)
Kondratko P. T., Greenhill L. J., Moran J. M. et al., 2006, ApJ, 638, 100 (Kondratko06)
Lo K. Y., 2005, ARA&A, 43, 625
Monet D., Levine S. E., Casian B. et al., 2003, AJ, 125, 984 (USNO)
Schlegel D. J., Finkbeiner D. P., Davis M., 1998, ApJ, 500,525
Schulz H., Henkel C., 2003, A&A, 400, 41
Tarchi A., Henkel C., Peck A. B. et al., 2002a, A&A, 385, 1049 (Tarchi02a)
Tarchi A., Henkel C., Peck A. B. et al. 2002b, A&A, 389, L39 (Tarchi02b)
Tarchi A., Henkel C., Chiaberge M. et al., 2003, A&A, 407, L33 (Tarchi03)
Tarchi A., Castangia P., Henkel C. et al., 2006, Mem.S.A.It.Suppl.10, 120
Zhang J. S., Henkel C., Kadler M. et al., 2006, A&A, 450, 933 (Zhang06)